

Modeling the EM Wave Interaction with the Body and SAR

Tamer S. Ibrahim (ibrahim@ou.edu)

School of Electrical and Computer Engineering and Bioengineering Center
University of Oklahoma, Norman, OK, United States

1. Introduction

The design of RF coils in MRI has traditionally been based on the use of circuit concepts [1] and transmission line theories [1,2], which invoke quasistatic field approximations [3]. At relatively low frequencies (< 3 Tesla applications), quasistatic approximations are valid for head coils because the RF coil is small compared to the wavelength of the RF field. At these operating frequencies, circuit concepts [3] can be applied to predict the resonance frequency and to determine the magnetic field by first assuming that the currents on the coil branches are uniform and then applying the Biot-Savart Law to determine the magnetic field produced by these currents.

Although the circuit model is a zero-dimensional approximation for the three-dimensional electromagnetic resonance behavior in the coil, it can be very accurate for modeling relatively complex coil geometries. At certain conditions however, these models start to fail because of two major limitations. First, the circuit model approximation breaks down when the coil geometry is a significant fraction of the wavelength. This limitation is not critical at 64 MHz, because the corresponding wavelength is 4.7 m. Thus, even the diameter of a body coil (approximately 0.8 m) is less than 20% of a wavelength. Even at high frequencies (200-300 MHz), analytical models [4,5] based on transmission line concepts and circuit models can still adequately describe the electromagnetic operation of empty head coils. However, these models start to fail as we look into 7 Tesla empty body coils. Second, as these analytical models start to breakdown with increasing frequency, they fail at a much faster rate with the presence of tissue. Tissue distorts the ideal and easily modeled (from an analytical point of view) transverse electromagnetic (TEM) field structure, which typically exist in low field operation, leading to hybrid modes instead. These hybrid modes are extremely challenging to model analytically.

With the failure of quasistatic approximations as the operational frequency increases, a computational tool based on full wave electromagnetics becomes essential in conducting feasibility studies and in designing and evaluating the performance of high-field RF coils.

2. Full Wave Electromagnetics in MRI: Background

Until the last decade, full-wave numerical methods have seldom been used to model the fields in RF coils for MRI systems. Before that, there was not much need for such an approach because most of the systems were at magnetic field strengths of 1.5 Tesla and below. In the last decade, however, there have been numerous applications of full-wave numerical methods to analyze a variety of RF coils. For instance, Han and Wright utilized a 2D finite difference time domain (FDTD) method to model surface MRI coils loaded with phantoms [6]. The FDTD method has also been used to analyze a head sized TEM resonator [7] loaded either with a phantom [7-9] or with a human head model [10-15]. The finite elements method (FEM) has also been used to approximate the specific absorption rate (SAR) inside the human head in a saddle shaped MRI head coil at 64 MHz [16]. In 1996, Jin et al. employed the conjugate gradient method with the fast Fourier transform to study the birdcage coil. Later, the FDTD method was also used to analyze the same problem [12,13,17-22]. In addition, simulations have made advancements to predict temperature distributions by thermal modeling [23-26]. Many of these full wave studies have shown excellent quantitative correlation with experimental data at 7 Tesla and 8 Tesla for surface [27,28] and volume head [8,29-31] coils. With so many full wave approaches available, an important question remains: which of these methods is mostly suited for modeling loaded high-field MRI RF coils?

3. The Finite Difference Time Domain Method

There are three main numerical methods used in electromagnetics: the finite element method (FEM), the finite difference time domain (FDTD) method, and the integral equation method, also known

as method of moments (MM). Although MM and FEM can be implemented in the time domain, they are rarely used in this way; rather, they are usually associated with the frequency domain. MM is fundamentally different from FEM and FDTD in that MM can be formulated in terms of unknown surface currents on perfect conductors and unknown volume currents in materials, whereas the unknowns in FEM and FDTD are the fields values everywhere within the volume of interest. Because of this, MM has great advantages over FDTD and FEM when it is applied to geometries consisting of only perfect conductors, since the number of unknowns in MM is much less than the other two methods.

For problems where large portions of the geometry are non-perfectly conducting, the number of unknowns for all three methods is comparable; however, the computation times vary greatly. Both MM and FEM require the solution of matrix equation. Since the number of unknowns required to model a coil is very large, iterative methods offer the only viable way to solve the matrix equation. Assuming the number of unknowns in the problem is N , the computation time is proportional to N^θ , where θ is 2 for MM and 1.5 for FEM. It should be noted that when there are large permittivity and conductivity contrasts in the geometry, which occurs when human tissue is present, the values for θ may be significantly larger than the nominal values given. On the other hand, the FDTD method does not require a matrix solution, and its computation time is proportional to $N^{4/3}$.

There is also a wide disparity in memory requirements between the three methods. The memory needed to solve an MM problem with 50,000 unknowns can be used to solve an FEM problem with 5,000,000 unknowns and an FDTD problem with 100,000,000 unknowns. The one disadvantage of FDTD compared to FEM is that it is less flexible for modeling arbitrary geometries, because FEM can be applied to unstructured grids. However, for the electrically large geometries that are encountered in high-field MRI, one can argue that FDTD is more appropriate than FEM, because in many cases, the number of unknowns needed to solve the problem is relatively very large. In addition, many tailored algorithms can be utilized to optimize the standard FDTD scheme. In fact, many such algorithms have been successfully applied for MRI simulations [32]. The next section will address: "How to build RF coil simulator (in-house or using commercial software) using the FDTD method?"

4. RF Coil Simulator Using the FDTD Method

The explicit FDTD technique introduced by Kane [33] is used to provide a direct solution for Maxwell's time-dependent curl equations. The FDTD method is essentially based on replacing the spatial and the time domain derivatives of Maxwell's equations with finite difference approximations. An excellent source for the FDTD formulation can be obtained from [34]. To create an FDTD model for MRI RF coil simulations, we will need an anatomically detailed human model (for the coil load) as well as a coil grid. In the following two sections, we will briefly discuss these tasks (a head coil simulation will be used as an example).

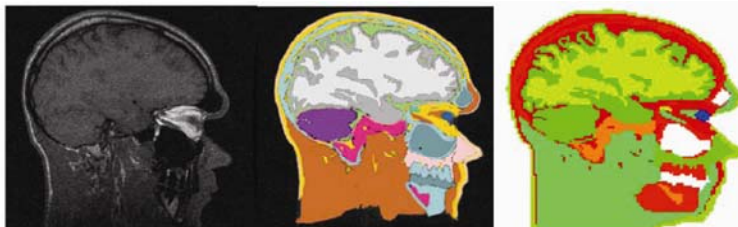
4.1. The Anatomically Detailed Human Head Model

With the availability of the visible human project anatomically detailed mesh (<ftp://starview.brooks.af.mil/EMF/dosimetry> models), is it necessary to develop new anatomically detailed models? To achieve general behavioral characteristics of the coil, the answer is most likely no. On the other hand, for precise comparisons between experiments and simulations or to achieve robustness in a coil design, i.e. acceptable performance with different coil loads, the answer is definitely yes.

An example of developing an anatomically detailed human head model is presented in [11]. The mesh data was obtained from 0.5mm x 0.5mm x 2mm 1.5 Tesla MRI images. The model was constructed by assigning tissue types in each image and then encoded these types on a digital image. Figure 1 describes the girding process [11,12]. Several error-correction and validation procedures were performed. First, the digitally encoded tissue types were processed to remove voids in the data caused by human error in tissue delineation. Erroneous voids were distinguished from true voids (air spaces in the mouth and nasal passages) and were filled by assigning an adjacent tissue type. Automated image processing software was developed to accomplish this task. Next, differences from layer to layer (image to image) in

the data set were reconciled by re-slicing the data along a different axis and re-examining the imagery to identify discontinuities in tissue boundaries. Some interpolation of the data was also required because of the difference in sample spacing within an image and between images. Finally, the image data were output as a single volumetric data set that specifies tissue types at each sample position. The tissue type information stored at each voxel is used with a look-up-table that provides dielectric constant and conductivity values for any frequency of interest.

Figure 1: The creation of the anatomically detailed human head model; left is the 1.5 Tesla image, center is the manually digitized grid, and right is the FDTD grid.



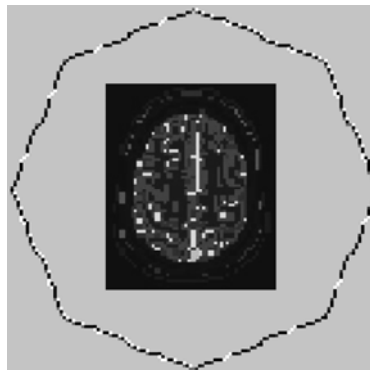
4.2. Model of the Coil Structure: How to Grid?

As we have created/used available anatomically detailed human models (the load), we will examine the needed steps for setting up the grid of the coil and the load followed by designing the FDTD source code (in case you are generating your own). In particular, we will look at examples using the birdcage [1] and the TEM [7] resonators.

4.2.1. The Birdcage Coil

In order to obtain accurate electromagnetic analysis of the birdcage coil operation with the FDTD algorithm, an octagonal geometry can be utilized in which the lumped capacitive elements are properly modeled. Figure 2 shows the FDTD coil grid, where eight-fold symmetry is maintained, and the human head. The different shaded points on the grid correspond to different algorithms utilized to describe the desired geometry. For instance, a lumped element FDTD algorithm is used to model the tuning capacitors [35]. This algorithm requires that the capacitive lumped elements be positioned along the Cartesian axes, namely x or y . Thus, in order to maintain symmetry, the orientation of the capacitors along the eight slanted edges of the rings may change. Another example is an FDTD algorithm which was utilized to model the curvatures [13] of the rings and strips, which removes stair-stepping errors from these critical coil components. To simulate quadrature excitation, the same excitation can be applied to two different drive points, as is done in experiment. The only difference between the two ports is a 90° relative phase shift on the input excitations. A differentiated Gaussian pulse can be used to excite the system [20-22].

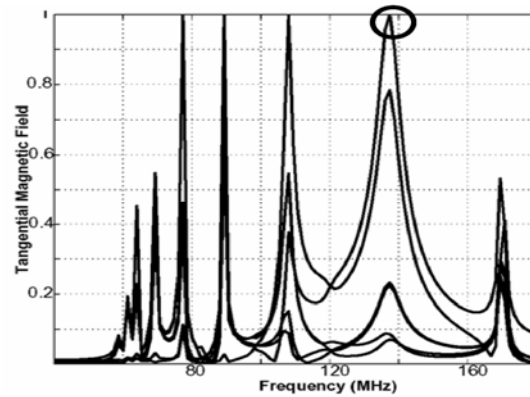
Figure 2: FDTD grid of the top circular ring of the birdcage coil. The different shadings on the grid correspond to different non-standard FDTD algorithms used to achieve an accurate representation of the physical performance of the coil. These include lumped capacitors and slanted non-cubical cells used to account for the curvature of the ring as well as the struts.



The electrical performance of the coil can be accurately predicted since the modeled geometry does not deviate greatly from the coil's actual shape. Figure 3 clearly demonstrates this point, in which an FDTD calculated frequency spectrum [30,36] of a 3 Tesla high pass birdcage coil that is numerically loaded with the visible human project head/shoulder anatomical mesh [37] is shown. The numerical values of the capacitors used along the end rings were set to the values of the actual lumped capacitors

used in the GE birdcage coil in clinical operation (15.5pF for 3 Tesla). First, the spectrum shows 9 modes corresponding to the 16 struts in the coil. Second, the resonance frequency of the “homogenous mode” of operation differs by less than 7.5 % from what is actually obtained in the real coil (128 MHz).

Figure 3: FDTD calculated frequency response of high-pass birdcage coil loaded with the head model. The capacitance value used was 15.5 pF (currently utilized for 3T operation). The spectrum shows 9 modes representing the 16-struts of the coil. The circle represents the linear mode of operation; its frequency is within 7.5 % of the experiment value.



4.2.2. The TEM Resonator

Analytical models based on multi-conductor transmission line theory [4,5] have accurately described the operation of empty TEM coils. They have shown that for an empty N-strut TEM coil, N/2+1 TEM modes exist. The second mode on the spectrum, mode 1, produces a linearly polarized field that can be utilized for imaging. The other modes produce nulls in the center of the coil, rendering them ineffective for conventional imaging.

Similar to the birdcage coil, the TEM resonator and the object to be imaged (phantoms or human head/body models) can be modeled as a single system with the FDTD method [8,10-13,15,38]. Figure 4 displays the FDTD grids of 16/32-strut TEM resonators loaded with the human head/body models. A stair-step approximation can be used to model the shield and the top and bottom rings of the coil. The coaxial rods can be modeled with a modified FDTD algorithm [13] that accounts for the curvatures of the rods to minimize errors caused by stair-stepping. To achieve rigorous modeling of the excitation port(s), the coil must be numerically tuned by adjusting the gap between the TEM stubs until any mode of interest is resonant at the desired frequency of operation. For a loaded coil, this process must be performed while the load is simultaneously present within the coil structure. Figure 8-5 presents the tuning process of the model by displaying a FDTD calculated frequency spectrum of a 16-strut TEM resonator (loaded with an 18.5-cm diameter spherical phantom filled with 0.125 M NaCl) and a corresponding experimentally measured S11 spectrum for the same coil dimensions and load.

Figure 4: 3D FDTD models of anatomically detailed human head/body models loaded within the TEM resonators.

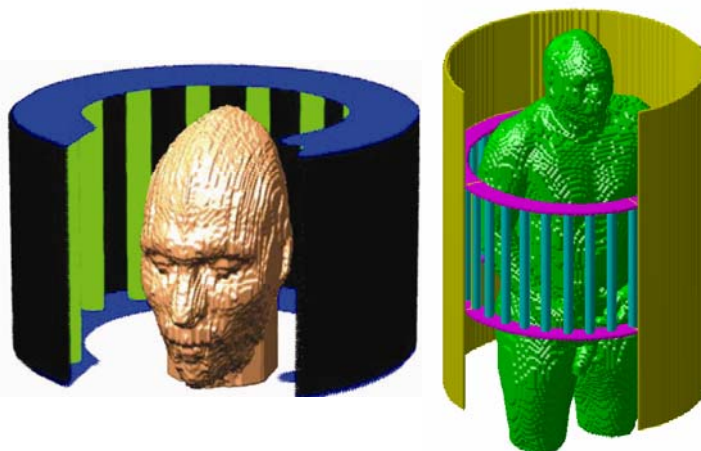
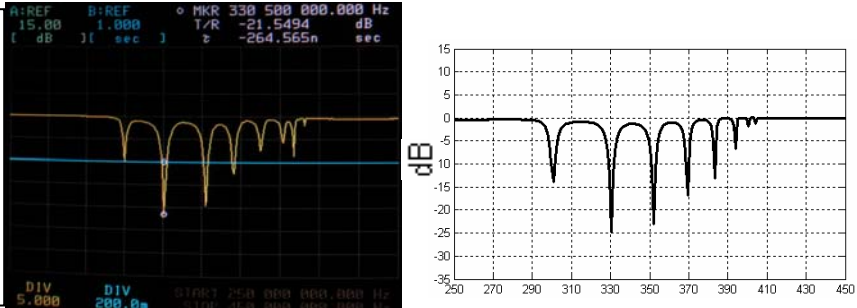


Figure 5: Measured and FDTD calculated response of a loaded (18.5-cm diameter spherical phantom filled with 0.125 M NaCl) 16-strut TEM resonator where the mode of operation is tuned to approx. 330 MHz.



4.2.3. Grid Size and Absorbing Boundary Conditions

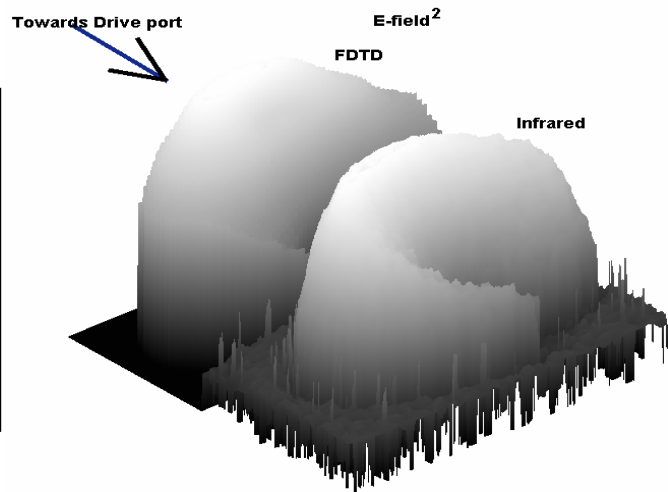
The resolution and therefore the size of problem is dependant on the needs of the modeler. A rule of thumb is the resolution must not be less than $(\lambda/20)$, where λ is the shortest wavelength in the problem. If the modeler is only interested in the general overall behavior of the coil without rigorously modeling the drive ports, feeding coaxial lines, and/or the tuning elements, the need for high resolution coil grids is not justified. On the other hand, if the modeler is interested in the coil's frequency response, input impedance, and localized SAR and B_1 effects, the aforementioned elements must be rigorously modeled and a high resolution is needed. For instance, 25,000,000/8,000,000 cells were used to generate the complete grid of the birdcage/TEM head coils.

The perfectly matched layer (PML) absorbing boundary condition [39] currently is considered to be the optimal method to absorb RF radiation from the coil. Typically, 16 layers (cells) on each side of the coil with about 10 cells separation between the PML surface and closest point on the coil geometry/load are needed.

4.3. Effects of Rigorous Source Modeling on the Electric Field

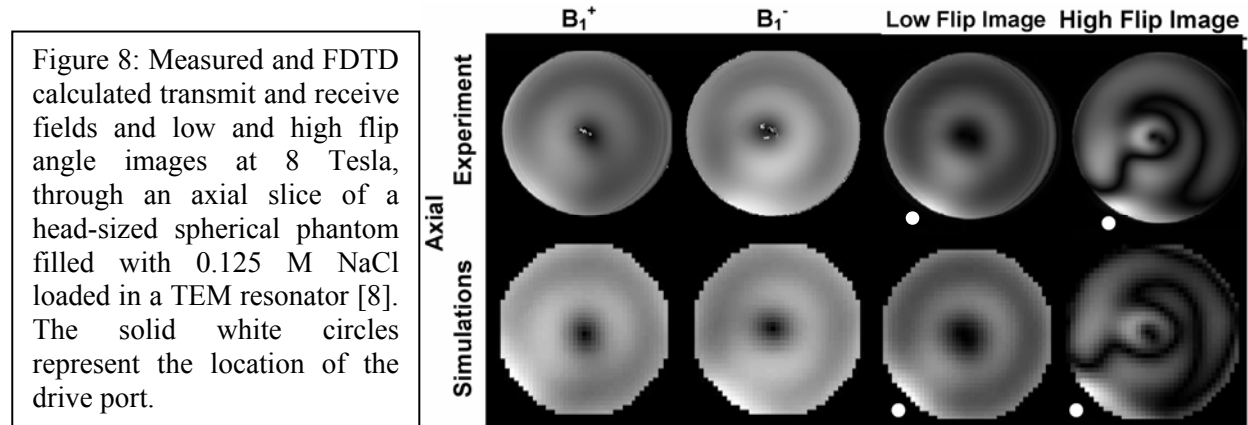
By exciting the coil in one location or multiple locations and allowing the coil currents to be properly calculated with Maxwell's equations, one can properly account for the coupling between the drive port and the object to be imaged. At high frequency, it is expected that this coupling will have a significant effect on the electric fields and therefore SAR values, particularly near the source. Figure 7 displays infrared-measured and FDTD-calculated square of transverse electric field distribution of an axial slice inside the spherically loaded 16-strut TEM resonator [40]. The resonator was experimentally and numerically excited at one port and tuned to 340 MHz. Excellent agreement is obtained between the FDTD and infrared results. It is also observed that one can clearly identify the location of the excitation source, which underscores the importance of modeling the source rigorously.

Figure 7: Infrared images and FDTD calculated transverse E-Field² distribution of an axial slice inside a loaded (18.5-cm diameter spherical phantom filled with 0.125 M NaCl) 16-strut TEM resonator. The resonator was tuned to 340 MHz and excited at one port.



4.4. Effects of Rigorous Source Modeling on the Magnetic Field

Effects of source modeling are not exclusively seen in electric field distributions, but also in magnetic fields distributions. Figure 8 shows axial measured transmit (B_1^+) and receive (B_1^-) fields, as well as low and high (1540 near the center of the phantom) flip angle images obtained at 8T, and the corresponding simulated results obtained at 340 MHz using the FDTD model, corresponding to mode 0 (first mode on the spectrum) [8]. The coil is a 16-strut TEM resonator, and the load utilized in the experiments and the numerical model is an 18.5-cm diameter sphere filled with 0.125 M NaCl. The solid white circle corresponds to the position of the excitation source [8]. It can be clearly seen that there is strong coupling (high signal intensity in the load near the source) between the excitation port and the phantom. This physical effect can clearly be accurately produced in simulation through rigorous modeling of the excitation port [8].



4.5. The FDTD Code

A general FDTD code for MRI RF coil simulations would start by dynamically allocating the memory requirements for all the arrays including electric field vectors, magnetic field vectors, permittivity, conductivity, and capacitance. With different coil geometries, cell sizes, and coil loading (empty, phantoms, or human head models), dynamic allocations provide convenience and conservation of memory. The next step is assigning the proper electrical properties to specific portions of the grid, including the phantom or the biological tissues of the human head model. The time loop then starts with no coil excitations implemented, so the initial field values are set to be zero. The time is then incremented by one time step, and the excitation is “turned on” at a specified excitation location. Note that the shape of the excitation is not important, as long as its frequency spectrum contains the frequencies of interest. The electric field values are then updated everywhere in the grid. A lumped element FDTD algorithm is used to model the tuning capacitors at their corresponding positions on the coil. Also, the electric field components which are tangent to a perfectly conducting surface (coil structure) are forced to zero. To avoid stair stepping errors, algorithms are used to model slanted perfect conductors. Using the calculated electric field values, the magnetic field values are then updated throughout the entire grid. This denotes the end of the time step. The time step procedure is then repeated until the simulation has run a prescribed number of time steps. Because the updated field values are only functions of the previous field values, memory is conserved. At any cell, memory conservation is accomplished by overwriting the updated field value into the same memory location which contains the previous value at the same cell.

In actuality, the goal is to obtain the electromagnetic field distribution within the coil at a specific frequency of interest (the appropriate Larmor frequency), after the coil’s mode of operation has been tuned to this frequency by adjusting the value of the lumped capacitors (birdcage coil) or the gap between inner struts (TEM coil). From the magnetic field distribution, one can extract the B_1 field distribution, and from the electric field distribution, one can determine the SAR as well as the total power absorbed by the phantom or the human head. Obtaining these field distributions is a two step process. In the first step, an

initial guess is made for the capacitor values (birdcage coil) or the gap between the inner struts (TEM coil). The coil is then excited and an FFT (Fast Fourier Transform) implementation is then applied to the FDTD solution at a few points within the grid to obtain a representation of the frequency response of the coil. The location of the points where the data is collected is not important, since the frequency components corresponding to different points within the coil should not differ significantly (the only difference should be variations in the magnitudes). If the resonance frequency of the coil's operational mode is not at the desired frequency, the capacitor values are changed or the gaps are adjusted, and the FDTD program is rerun. This step is repeated until the mode of interest resonates at the desired frequency. In the second step, the FDTD solution is run with the correct capacitor values or gap sizes, but instead of applying an FFT at a few points in the grid, a DFT (discrete Fourier transform) is applied on-the-fly at all points of interest within the grid at the resonant frequency. Thus, the time domain data does not need to be stored, and the coil's field distribution is known at the appropriate resonant frequency.

5. Reference List

- [1] Hayes, E. C., Wdelstein, W. A., Schenck, D. F., Mueller, O. M. , and Eash, M., An efficient highly homogeneous radiofrequency coil for whole-body NMR imaging at 1.5 T *Journal of Magnetic Resonance*, vol. 63, pp. 622-628 , 1985.
- [2] Glover, H., Hayes, C. E., Pelc, N. J., Edelstein, W. A., Mueller, O. M., Hart, H. R., Hardy, C. J., O'Donnell, M., and Barber, W. D., Comparison of Linear and Circular Polarization for Magnetic Resonance Imaging *Journal of Magnetic Resonance*, vol. 64, pp. 255-270, 1985.
- [3] Tropp, J., The theory of the bird-cage resonator *J. Magn. Reson.*, vol. 82, pp. 51-62, 1989.
- [4] Baertlein, B. A., Ozbay, O., Ibrahim, T. S., Yu, Y., Lee, R., Kangarlu, A., and Robitaille, P.-M. L., Theoretical model for an MRI radio frequency resonator *IEEE Bio Med. Eng.*, vol. 47, pp. 535-546, 2000.
- [5] Bogdanov, G. and Ludwig, R., Coupled microstrip line transverse electromagnetic resonator model for high-field magnetic resonance imaging *Magn Reson Med*, vol. 47, pp. 579-93, Mar, 2002.
- [6] Han, Y. and Wright, S. M., Analysis of RF Penetration Effects in MRI Using Finite-Difference Time-Domain Method *In the Proceeding of Annual Meeting of ISMRM, New York, NY*, p 1327. 1993.
- [7] Vaughan, J. T., Hetherington, H. P., Otu, J. O., Pan, J. W., and Pohost, J. M., High frequency volume coils for clinical NMR imaging and spectroscopy *Magnetic Resonance in Medicine*, vol. 32, pp. 206-218 , 1994.
- [8] Ibrahim, T. S., Mitchell, C., Lee, R., Schmalbrock, P., and Chakeres, D. W., Perspective into The Operation of RF Coils from 1.5 to 11.7 Tesla *Magn Reson Med*, vol. 54, pp. 683-690, 2005.
- [9] Kangarlu, A., Ibrahim, T. S., and Shellock, F. G., Effects of coil dimensions and field polarization on RF heating inside a head phantom *Magn Reson Imaging*, vol. 23, pp. 53-60, Jan, 2005.
- [10] Ibrahim, T. S., Abduljalil, A. M., Lee, R., Baertlein, B. A., and Robitaille, P.-M. L., Analysis of B1 field profiles and SAR values for multi-strut transverse electromagnetic RF coils in high field MRI application. *Physics in Medicine and Biology*, vol. 46, pp. 2545-2555 , 2001.
- [11] Ibrahim, T. S., Lee, R., Baertlein, B. A., and Robitaille, P.-M. L., Effect of RF Coil Excitation on Field Inhomogeneity at Ultra High Fields: A Field Optimized TEM Resonator *Magnetic Resonance Imaging*, vol. 19, pp. 1339-1347, 2001.
- [12] Ibrahim, T. S., Lee, R., Abduljalil, A. M., Baertlein, B. A., and Robitaille P.-M.L., Calculations of EM interactions with biological tissue: magnetic resonance Imaging at ultra high field *Applied Computational Electromagnetics*, vol. 16, pp. 138-144 , 2001.
- [13] Ibrahim, T. S., Lee, R., Abduljalil, A. M., Baertlein, B. A., and Robitaille, P.-M. L., Dielectric resonances and B₁ field inhomogeneity in UHFMRI: computational analysis and experimental findings *Magnetic Resonance Imaging*, vol. 19, pp. 219-226, 2001.
- [14] Vaughan, J. T., Garwood, M., Collins, C. M., Liu, W., DelaBarre, L., Adriany, G., Andersen, P., Merkle, H., Goebel, R., Smith, M. B., and Ugurbil, K., 7T vs. 4T: RF power, homogeneity, and signal-to-noise comparison in head images *Magn Reson Med*, vol. 46, pp. 24-30, Jul, 2001.
- [15] Ibrahim, T. S., A numerical analysis of radiofrequency power requirements in magnetic resonance imaging experiments *IEEE Transactions on Microwave Theory and Techniques special issue on Biological Effects and Medical Applications of RF/Microwaves* , vol. 52, pp. 1999-2003 , 2004.
- [16] Simunic, D., Watch, P., Renhart, W., and Stollberger, R., Spatial Distribution of High-Frequency Electromagnetic Energy in Human Head During MRI: Numerical Results and Measurements *IEEE Trans. Biomedical Eng.*, vol. 43, pp. 88-94, 1996.
- [17] Collins, C. M., Li, S., and Smith, M. B., SAR and B1 field distributions in a heterogeneous human head

- model within a birdcage coil. Specific energy absorption rate *Magn Reson Med*, vol. 40, pp. 847-56, 1998.
- [18] Chen, J., Feng, Z., and Jin, J. M., Numerical simulation of SAR and B1-field inhomogeneity of shielded RF coils loaded with the human head *IEEE Trans. Biomedical Eng.*, vol. 45, pp. 650-659, 1998.
- [19] Gandhi, O. P. and Chen, X. B., Specific absorption rates and induced current densities for an anatomy-based model of the human for exposure to time-varying magnetic fields of MRI *Magn Reson Med*, vol. 41, pp. 816-23, 1999.
- [20] Ibrahim, T. S., Lee, R., Baertlein, B. A., Kangarlu, A., and Robitaille, P.-M. L., Application of finite difference time domain method for the design of birdcage RF head coils using multipoint excitations *Magnetic Resonance Imaging*, vol. 18, pp. 733-742, 2000.
- [21] Ibrahim, T. S., Lee, R., Baertlein, B. A., Yu, Y., and Robitaille, P.-M. L., Computational analysis of the high pass birdcage resonator: Finite difference time domain simulations for high-field MRI *Magnetic Resonance Imaging*, vol. 18, pp. 835-843, 2000.
- [22] Ibrahim, T. S., Lee, R., Baertlein, B. A., and Robitaille, P.-M. L., B1 Field Homogeneity and SAR Calculations in the High Pass Birdcage Coil *Physics in Medicine and Biology*, vol. 46, pp. 609-619, 2001.
- [23] Collins, C. M., Smith, M. B., and Turner, R., Model of local temperature changes in brain upon functional activation *J Appl Physiol*, vol. 97, pp. 2051-5, Dec, 2004.
- [24] Trakic, A., Crozier, S., and Liu, F., Numerical modeling of thermal effects in rats due to high-field magnetic resonance imaging (0.5-1 GHz) *Phys Med Biol*, vol. 49, pp. 5547-58, Dec 21, 2004.
- [25] Hand, J. W., Lau, R. W., Lagendijk, J. J., Ling, J., Burl, M., and Young, I. R., Electromagnetic and thermal modeling of SAR and temperature fields in tissue due to an RF decoupling coil *Magn Reson Med*, vol. 42, pp. 183-92, 1999.
- [26] Cline, H., Mallozzi, R., Li, Z., McKinnon, G., and Barber, W., Radiofrequency power deposition utilizing thermal imaging *Magn Reson Med*, vol. 51, pp. 1129-37, Jun, 2004.
- [27] Collins, C. M., Yang, Q. X., Wang, J. H., Zhang, X., Liu, H., Michaeli, S., Zhu, X. H., Adriany, G., Vaughan, J. T., Anderson, P., Merkle, H., Ugurbil, K., Smith, M. B., and Chen, W., Different excitation and reception distributions with a single-loop transmit-receive surface coil near a head-sized spherical phantom at 300 MHz *Magn Reson Med*, vol. 47, pp. 1026-8, May, 2002.
- [28] Wang, J., Yang, Q. X., Zhang, X., Collins, C. M., Smith, M. B., Zhu, X. H., Adriany, G., Ugurbil, K., and Chen, W., Polarization of the RF field in a human head at high field: a study with a quadrature surface coil at 7.0 T *Magn Reson Med*, vol. 48, pp. 362-9, Aug, 2002.
- [29] Ibrahim, T. S., Mitchell, C., Schmalbrock, P., and Chakeres, D. W., The TEM Resonator modes: A study at high field MRI' *In The Proceedings of The Annual Meeting of ISMRM, Toronto, Canada*, p. 2553, 2003.
- [30] Ibrahim, T. S. and Lee R., Specific absorption rate at 1.5T and 3T: a numerical study of the birdcage coil *In The Proceedings of The Annual Meeting of ISMRM, Toronto, Canada*, p 2602, 2003.
- [31] Ibrahim, T. S., Mitchell, C., Schmalbrock, P., and Chakeres, D. W., Computational and Experimental Analysis of Electromagnetic Fields Induced by RF Coils for High Field Imaging *In The Proceedings of The Annual Meeting of ISMRM, Kyoto, Japan*, p 488. 2004.
- [32] Wei, Q., Liu, F., Xia, L., and Crozier, S., An object-oriented designed finite-difference time-domain simulator for electromagnetic analysis and design in MRI--applications to high field analyses *J Magn Reson*, vol. 172, pp. 222-30, Feb, 2005.
- [33] Yee, K. S., *Numerical solutions of the initial boundary value problems involving Maxwell's equations in isotropic media* *IEEE Trans. Ant Prop*, vol. 14, pp. 302-317, 1966.
- [34] Taflove, A. and Hagness, S. C., *Computational Electrodynamics The Finite Difference Time Domain Method* Anonymous2000. Artech House. Boston.
- [35] Tsuei, Y., Cangellaris, A. C., and Prince, J. L., Rigorous electromagnetic modeling of chip-to-package (first-level) interconnections *IEEE Trans. Com. Hybrids Manuf*, vol. 16, pp. 876-882, 1993.
- [36] Ibrahim, T. S. and Lee R., Effects of Geometry, excitation and spatial positioning on the birdcage coil performance *In The Proceedings of The Annual Meeting of ISMRM, Toronto, Canada*, p 2518, 2003.
- [37] Gabriel, C. Compilation of dielectric properties of body tissues at RF and microwave frequencies. 96.
- [38] Ibrahim, T. S., Kangarlu, A., and Chakeres, D. W., Design and Performance Issues of RF coils utilized in Ultra High Field MRI: Experimental and Numerical Evaluations. *IEEE Bio Med. Eng.*, vol. 52, pp. 1278-1284, 2005.
- [39] Berenger, J. P., A perfectly matched layer for the absorption of electromagnetic waves *Journal of Computational Physics*, vol. 114, pp. 185-200, 1994.
- [40] Ibrahim, T. S. and Lee, R., Evaluation of MRI RF Probes Utilizing Infrared Sensors *IEEE Transactions on Biomedical Engineering*. In press.